



Cite this: *RSC Adv.*, 2024, 14, 5055

Nitrogen-doped carbon material NCM-*T* heterogeneously catalyzed liquid-phase hydrogenation of nitrobenzene to aniline

Wenxiu Gao,^a *^a Yongping Gao,^a Bai Liu,^a Jianing Kang,^a Zhihui Zhang,^a Min Zhang^a and Yongcun Zou^b

As an important chemical intermediate, aniline is primarily produced industrially through catalytic hydrogenation of nitrobenzene. Herein, a series of nitrogen-doped carbon materials (referred to as NCM-*T*, with *T* denoting the roasting temperature (°C)) were prepared through high-temperature roasting of sucrose and melamine for the heterogeneous catalytic liquid-phase hydrogenation of nitrobenzene to aniline. A preliminary study of the involved reaction mechanism was performed by combining the results of material characterisation and catalyst evaluation. Experimental results showed that the graphitic N content and the defective sites simultaneously affected the performance of NCM-*T* in catalysing the hydrazine hydrate reduction in the nitrobenzene hydrogenation reaction. The catalyst NCM-800 was reacted in an ethanol solution with hydrazine hydrate as the reducing agent at 80 °C for 5 h. Notably, the nitrobenzene conversion rate was up to 94%, and the aniline selectivity was 100%. The turnover frequency (TOF) could reach up to 7.9 mol g⁻¹ h⁻¹, and after five recycling cycles, only a small loss of catalytic activity was observed. This shows that the prepared catalyst is a recyclable catalyst that can be used for reducing the nitrobenzene from hydrazine hydrate to aniline.

Received 4th January 2024
Accepted 1st February 2024

DOI: 10.1039/d4ra00078a

rsc.li/rsc-advances

Introduction

Aniline is an important intermediate in syntheses of organic chemical raw materials that are widely used in organic dyes, pesticides, pharmaceuticals and textiles.^{1–7} Nitrobenzene hydrogenation is a common method for industrial aniline production. Traditional metal catalysts generally have high catalytic activity, but often have poor stability and cannot be reused.^{8–10} The development of efficient heterogeneous metal-free catalysts for nitrobenzene-reduction is inexpensive, environment-friendly and stable, thereby meeting the needs of industrial development; furthermore, it has market application potential.

The application of carbon materials in the field of catalysis has recently garnered attention.^{11–17} However, the uniform charge distribution and inertness of carbon materials weaken their interaction with reactants, limiting their application as catalysts. Surface functionalization, doping with heteroatoms, and defects creation are the most commonly employed strategies for improving the catalytic properties of carbon materials. Compared to the synthesis of nitrogen-doped carbon nano-materials through post-treatment, the *in situ* synthesis of

nitrogen-rich organic backbone materials *via* high-temperature carbonisation results in better dispersion and stability of nitrogen functional groups in the materials; this is more conducive to improving the catalytic activity and stability of materials.^{18,19} In case of electron-rich nitrogen-doped carbon materials, the π -electrons of carbon are activated *via* conjugation with the lone-pair electrons of nitrogen, resulting in excellent catalytic activity. After high-temperature roasting, numerous locally charged defect sites are generated and transferred to the involved reactants, activating the reactants and further promoting the catalytic reaction.^{20–22}

Zhang *et al.*²³ prepared a nitrogen-doped carbon material (labeled as NC-*T*) for the catalytic reduction of nitro compounds by hydrazine hydrate *via* thermal treatment of a melamine-chitosan composite; the catalytic activity enhanced with increasing the pyrolysis temperature cause the enhanced ratio of graphitic-type nitrogen in NC-*T*. This confirmed that graphitic-type nitrogen is an active site for promoting the reduction of nitro compounds. Dong *et al.*²⁴ prepared a renewable N-doped carbon material (RNC) derived from soybean pulp for catalysing the chemoselective hydrogenation reaction of halogenated nitrobenzenes; their results showed that the defective sites around the pyrrolic N and pyridinic N in RNC enhanced the electron density, which was conducive to the promotion of the nitro group's protonation as an active site for the hydrogenation reaction. Li *et al.*²⁵ employed melanin or protoporphyrin IX as a dopant and effectively controlled the content of doped graphitic nitrogen by

^aCollege of Chemistry and Pharmaceutical Engineering, Jilin Institute of Chemical Technology, Jilin 132000, China. E-mail: gaowenxiu-0922@jlicet.edu.cn

^bState Key Laboratory of Inorganic Synthesis and Preparative Chemistry, College of Chemistry, Jilin University, Changchun 130012, China


varying the pyrolysis heating rate to obtain several nitrogen-doped carbon nanotubes (NCNTs); further, they employed these NCNTs to catalyse the hydrogenation of various nitroarenes, wherein graphitic N substantially affected the catalytic hydrogenation activity. Meanwhile, pyridinic N did not considerably affect the hydrogenation activity. Luo *et al.*²⁶ prepared nitrogen-doped carbon materials containing different nitrogen species for the catalytic hydrogenation of nitrobenzene to aniline using *in situ* synthesis and post nitridation treatment. Density functional theory calculations demonstrated that pyrrolic N in the nitrogen-doped carbon nanotubes was the key active centre for hydrogen activation *via* chemisorption and dissociation. However, the defective sites in the materials, *i.e.* pyridinic N and graphitic N, did not substantially contribute to the hydrogenation activity. Han *et al.*²⁷ prepared nitrogen-doped carbon material (NCS) *via* pyrolysis of β -cyclodextrin and urea for catalysing the nitrobenzene reduction reaction. The graphitic N formed *via* pyrolysis was the active site of the catalyst. The catalyst with a large graphitic nitrogen content and a high degree of defects exhibited excellent catalytic activity for reducing nitro compounds. Li *et al.*²⁸ prepared a series of nitrogen-doped carbon-based catalysts by selecting chitosan and dicyandiamide as precursors for catalysing the selective hydrogenation reaction of nitrobenzene with formic acid. Graphitic N was conducive to the adsorption of nitrobenzene molecules, while pyridinic N facilitated the activation of formic acid; thus, the synergistic effect of pyridinic N and graphitic N resulted in the formation of catalysts with excellent catalytic performance.

Although researchers have investigated the catalytic hydrogenation reduction of nitroaromatics by nitrogen-doped carbon materials, the relation between the conformation of nitrogen species that play a key role in the reaction and the catalytic activity remains unclear. However, this relation is crucial for further improving the catalytic activity, selectivity and stability. To this end, we prepared a series of nitrogen-doped carbon materials (referred to as NCM-*T*, where *T* denotes the roasting temperature (°C)) through *in situ* synthesis based on high-temperature roasting of melamine and sucrose for catalytic liquid-phase hydrogenation of nitrobenzene. We aimed to investigate the contribution of the configurations of nitrogen in the nitrogen-doped materials to the catalytic activity in the hydrogenation reduction reaction of nitroaromatics.

Experimental

Material synthesis

All chemicals are of analytical grade and were directly used without any further purification. In a typical synthesis procedure for NCM-*T*, sucrose (2.00 g) and melamine (8.00 g) were dissolved in deionized water (30 mL), stirred at 25 °C for 30 min and transferred to a 50 mL Teflon-lined autoclave. Subsequently, the obtained mixture was placed in a high-temperature oven to react at 200 °C for 8 h. The resultant was naturally cooled, filtered and washed with deionised water and ethanol several times. Thereafter, the product was dried and milled to obtain a brown NCM powder, which was roasted in a tube

furnace at a high temperature of *T* (*T* = 700, 800, 900) in a nitrogen atmosphere for 2 h to obtain NCM-*T*.

Catalyst characterisation

The morphologies of materials were observed through scanning electron microscopy (SEM; JSM-7610F Plus). X-ray diffraction (XRD) patterns were obtained using a D8 diffractometer with Cu- $\kappa\alpha$ radiation in the 2θ range of 10°–80°. Raman spectra were obtained using a Raman spectrometer (Raman) type INVIA. The elemental composition and bonding information of the samples were investigated *via* X-ray photoelectron spectroscopy (XPS; model ESCALAB 250). The specific surface area of the materials was determined using an ASAP 2020 Plus instrument.

General procedure

Nitrobenzene (0.5 mmol), solvent (4 mL), $\text{N}_2\text{H}_4 \cdot \text{H}_2\text{O}$ (3–5 mmol) and NCM-*T* (10–20 mg) were added to a 10 mL round-bottom flask fitted equipped with a reflux condenser, and the mixture was stirred for a certain time at 60 °C–80 °C. After the reaction, nitrobenzene conversion and aniline selectivity were determined *via* gas chromatography (GC 9790II; flame ionization (FID) detector; HP-5 capillary column; nitrogen as carrier gas).

Results and discussion

Characterisation of catalysts

Fig. 1 illustrates the XRD patterns of NCM and NCM-*T*. After high-temperature roasting, the periodicity of the NCM crystal structure was destroyed, resulting in the formation of more defects. The two broad peaks observed at 23° and 44° were assigned to the (002) and (100) crystal planes of graphitic carbon, respectively, this indicating that the material had a low graphitization degree. Among the materials, NCM-700 had more defects and NCM-900 had a slightly higher degree of graphitisation.

Fig. 2 shows the SEM images of NCM and NCM-*T*. As shown, the NCM samples appeared to have a thick folded laminar structure. Notably, the laminar structure of the NCM-*T* samples became thinner after high-temperature roasting and exhibited petal-like laminar morphology.

The N_2 adsorption–desorption isotherms and pore distribution curves of NCM and NCM-*T* are shown in Fig. 3. Both

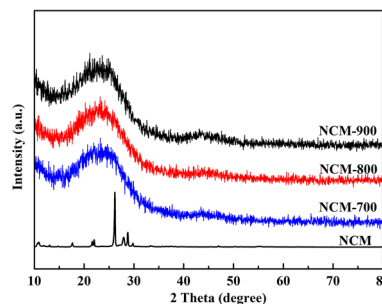
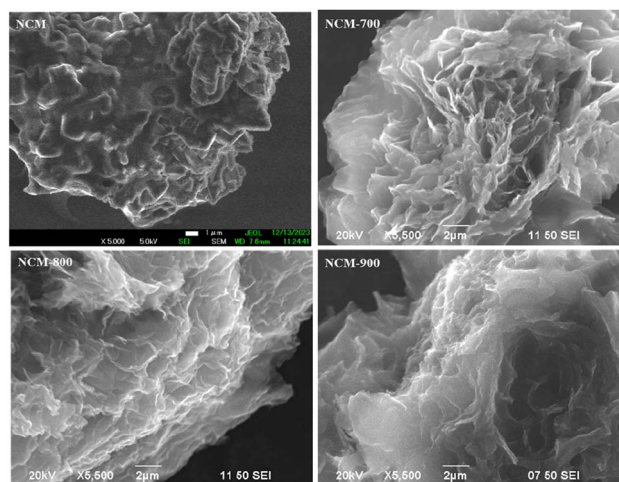
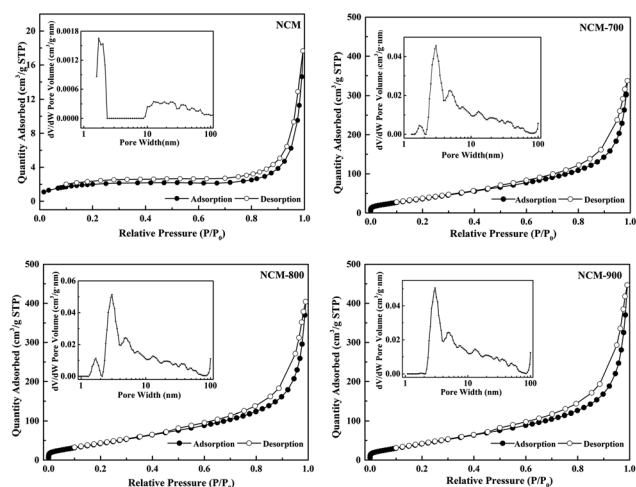


Fig. 1 The XRD pattern of NCM and NCM-*T*.



Fig. 2 The SEM images of NCM and NCM-*T*.Fig. 3 N₂ adsorption–desorption isotherms of NCM and NCM-*T*, and the corresponding pore size distribution curves (inset).

NCM and NCM-*T* conformed to the type-IV isotherm characteristics and exhibited a hysteresis loop. The pore distribution curves indicate that the optimal pore size of NCM-*T* was approximately 3 nm, which was in the mesoporous range. The values of the Brunauer–Emmett–Teller (BET) surface area, pore volume, and average pore size are summarized in Table 1. The pore volume and pore size of NCM considerably increased after roasting, while the pore volume and pore size of NCM-*T*

Table 1 The Physical properties of NCM and NCM-*T*

Entry	Samples	BET surface area (m ² g ^{−1})	Pore volume (cm ³ g ^{−1})	Average pore size (nm)
1	NCM	7	0.022	12.6
2	NCM-700	153	0.52	13.62
3	NCM-800	177	0.63	14.16
4	NCM-900	176	0.69	15.70

gradually increased with increasing roasting temperature. The specific surface area of NCM-800 was comparable to that of NCM-900, which might be because a larger pore volume and pore size of NCM-900 decreased the number of pores and subsequently led to a decrease in the specific surface area.²⁹

Fig. 4a presents the Raman spectra of NCM-*T*. The G band observed at 1580 cm^{−1} is attributed to the diffraction peaks of sp² hybridised graphitic carbon,³⁰ the D band observed at 1350 cm^{−1} is associated with the disordered or defective structure of the carbon atoms. The intensity ratio of the two peaks (IG/ID) indicates the graphitisation degree of carbon and the degree of defects in the material. The IG/ID ratios for NCM-700, NCM-800, and NCM-900 are 0.94, 0.97, and 1.04, respectively. This indicates a higher graphitisation degree in NCM-900 and a higher degree of defects in NCM-700; these results are consistent with the XRD results presented in Fig. 1. Defective sites can modulate the surface and electronic properties of catalysts and thus affect their catalytic activity.^{27,31} Fig. 4b–f present the full XPS spectra as well as the N 1s spectra of NCM and NCM-*T*. The full XPS spectra of NCM and NCM-*T* indicate the presence of C, N, and O. The high-resolution N 1s spectrum of NCM exhibits three peaks, with binding energies ranging from high to low corresponding to graphitic N, pyrrolic N, and pyridinic N. Furthermore, the high-resolution N 1s spectrum of NCM-*T* exhibits four peaks, corresponding to oxidized N, graphitic N, pyrrolic N and pyridinic N.

Table 2 lists the contents of nitrogen species in NCM and NCM-*T* determined through XPS. As shown, after roasting NCM at high temperatures, the overall nitrogen content in the

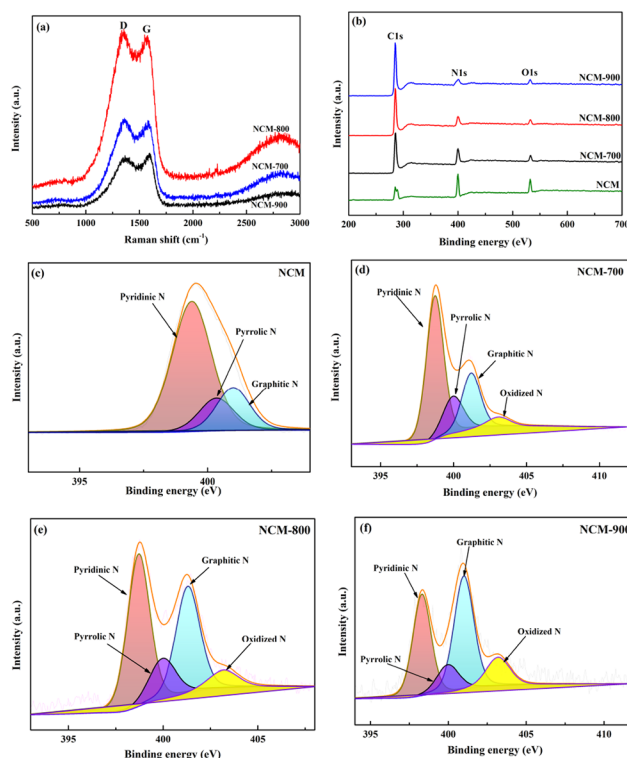


Fig. 4 Raman (a) and XPS (b–f) spectra.



Table 2 Analysis of nitrogen species content in NCM and NCM-T

Sample	N (%)	Nitrogen species (%)			
		Pyridinic	Pyrrolic	Graphitic	Oxidized
NCM	36.62	67	15	19	0
NCM-700	19.58	55	17	23	5
NCM-800	13.98	45	14	34	7
NCM-900	7.16	34.5	11.5	42	12

material decreases and the contents of pyridinic N and pyrrolic N decrease. Furthermore, the graphitic N content increases with increasing roasting temperature. This is because the pyridinic N and pyrrolic N with poor thermal stability are converted into the more stable graphitic N at high temperatures.³² A combined analysis of the overall content of nitrogen and the content of nitrogen species shows that NCM-800 has the highest graphitic N content.

Catalyst evaluation

Optimisation of the reaction conditions for the NCM-T catalysed nitrobenzene hydrogenation reaction is shown in Table 3. In a blank experiment with hydrazine hydrate as the reductant, the nitrobenzene conversion was only 5%. No change in nitrobenzene conversion was observed when the NCM samples were added as catalysts under the same conditions. Adding NCM-T under the same conditions resulted in a considerable increase in the nitrobenzene conversion, indicating that NCM-T played a catalytic role. The experimental factors such as roasting temperature, reducing agent dosage, catalyst dosage, reaction temperature and reaction solvent were examined. Notably, the roasting temperature exerted the greatest influence on nitrobenzene conversion, and NCM-800 exhibited the best catalytic effect. Based on the aforementioned results as well as the characterisation results, it can be speculated that the graphitic N content and the number of defective sites

simultaneously affect the performance of NCM-T in catalysing the reduction of nitrobenzene by hydrazine hydrate.³³

Mechanism discussion

The mechanism of nitrogen-doped carbon materials in catalysing nitrobenzene hydrogenation to aniline has been reported. However, the relation between the involved nitrogen species and catalytic performance needs further investigation.

The mechanism of heterogeneous NCM-T in catalysing liquid-phase nitrobenzene hydrogenation to aniline is speculated as in Fig. 5. Owing to the increased roasting temperature, some pyridinic N and pyrrolic N are converted into graphitic N. The graphitic N in the catalyst combines with the hydrogen in the hydrazine hydrate to form the N-H bond; simultaneously, the graphitic carbon near the graphitic N combines with the nitrogen atoms in hydrazine hydrate to form the C-N bond. Furthermore, hydrogen atoms are released *via* the cleavage of N-H bonds, which form C-H bonds with graphitic carbon. After this release of hydrogen atoms, the obtained intermediate H-N=N-H and hydrogen protons attack the -NO₂ in nitrobenzene adsorbed around the defects and the graphitic N; moreover,

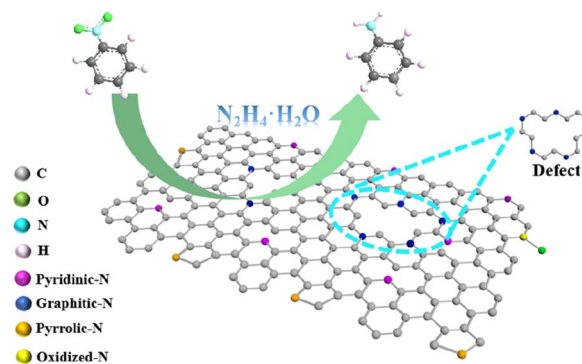


Fig. 5 Reaction mechanism for the hydrogenation of nitrobenzene catalyzed by NCM-T catalyst.

Table 3 Optimisation of reaction conditions for NCM-T catalysed hydrogenation of nitrobenzene^a

Entry	Catalysts (mg)	$n(\text{Nitrobenzene}) : n(\text{hydrazine hydrate})$	Temp. (°C)	Solvent	Conv. (%)	TOF ^b × 10 ⁻³ (mol g ⁻¹ h ⁻¹)
1	Blank	1 : 10	80	Ethanol	5	0.3
2	NCM/15 mg	1 : 10	80	Ethanol	5	0.3
3	NCM-700/15 mg	1 : 10	80	Ethanol	26	1.7
4	NCM-800/15 mg	1 : 10	80	Ethanol	94	6.3
5	NCM-900/15 mg	1 : 10	80	Ethanol	59	4.0
6	NCM-800/10 mg	1 : 10	80	Ethanol	79	7.9
7	NCM-800/20 mg	1 : 10	80	Ethanol	100	5
8	NCM-800/15 mg	1 : 6	80	Ethanol	44	3.0
9	NCM-800/15 mg	1 : 8	80	Ethanol	66	4.4
10	NCM-800/15 mg	1 : 10	70	Ethanol	45	3.0
11	NCM-800/15 mg	1 : 10	60	Ethanol	29	1.9
12	NCM-800/15 mg	1 : 10	80	Cyclohexane	79	5.3
13	NCM-800/15 mg	1 : 10	80	Toluene	54	3.6

^a Reaction conditions: 0.5 mmol nitrobenzene, 5 mmol hydrazine hydrate at a molar ratio of 1 : 10, both reaction times 5 h, the experimental data for catalytic evaluation were averaged over three repetitions to obtain. ^b TOF = mole of converted nitrobenzene/(mass of catalyst × reaction time).



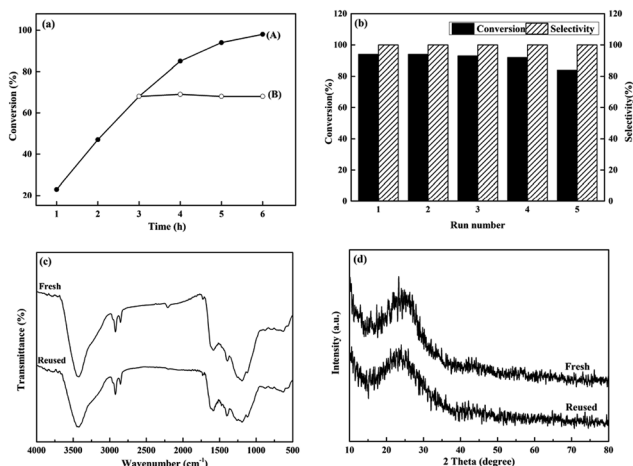


Fig. 6 (a) Interruption and (b) cycling experiments; (c) FTIR and (d) XRD spectra of NCM-800 before and after 5 cycles. Reaction conditions are the same as in Table 3, entry 4.

a reduction reaction occurs to produce aniline.³⁴ Both the defects formed in NCM-*T* after high-temperature roasting and the graphitic N promote nitrobenzene conversion to aniline.

Stability and recyclability

The stability of the NCM-800 catalyst was examined *via* interruption (Fig. 6a) and cycling experiments (Fig. 6b). In Fig. 6a, curve A shows a plot of nitrobenzene conversion as a function of reaction time. Curve B shows a plot of nitrobenzene conversion as a function of reaction time after filtering the catalyst while it was hot after 3 h of the reaction. No distinct change was observed in the nitrobenzene conversion before and after the interruption of the reaction. NCM-800 maintained a nitrobenzene conversion rate of 84–94% after five cycles (5 h per reaction, Fig. 6b). The catalyst structure did not considerably change after the cyclic reaction (Fig. 6c and d), indicating that NCM-800 is recyclable.

Conclusions

Herein, the relation between the nitrogen species in N-doped carbon materials and the performance of these materials in the catalytic hydrogenation reaction of nitrobenzene was investigated. A series of N-doped carbon materials, NCM-*T*, were prepared through high-temperature roasting *via in situ* doping. As the roasting temperature increased, more nitrogen species converted to graphitic N. The graphitic N and defective sites in the materials simultaneously promoted the conversion of hydrazine hydrate-reduced nitrobenzene to aniline. Overall, the results of this research provide design ideas for further developing high-performance aromatic hydrogenation catalysts without metal participation.

Author contributions

Wenxiu Gao: conceptualization, formal analysis, writing – review & editing, funding acquisition. Yongping Gao: data

curation, formal analysis, writing – original draft. Bai Liu: visualization. Jianing Kang: visualization, investigation. Zhihui Zhang: investigation. Min Zhang: investigation. Yongcun Zou: resources.

Conflicts of interest

There are no conflicts to declare.

Acknowledgements

This work was funded by Project of Science and Technology Development of Jilin Province (No. 2020122373JC), and the Jilin Provincial Education Department Scientific Research Planning Project (No. JJKH20200240KJ). Testing support received from the State Key Laboratory of Inorganic Synthesis and Preparative Chemistry of Jilin University, and JLICT Center of Characterization and Analysis are also acknowledged.

References

- 1 J. W. Guo, H. M. Liu, Y. Q. Li, D. Z. Li and D. H. He, *Front. Chem.*, 2023, **11**, 116283.
- 2 C. Doudou, S. Yao, Y. Yuchen, S. Xingfu, Z. Xiuqing, W. Xueguang and L. Xionggang, *Colloids Surf., A*, 2023, **665**, 131201.
- 3 J. J. Li, Z. Z. Wang, Y. R. Ma, C. Y. Xu and S. H. Zhou, *ACS Omega*, 2023, **8**, 12339–12347.
- 4 G. F. Liu, C. J. Chen and J. J. Chen, *J. Phys. Chem. C*, 2023, **127**, 4375–4386.
- 5 A. T. Nguyen and H. K. Kim, *RSC Adv.*, 2023, **13**, 31346–31352.
- 6 H. Liao, P. Q. Weng, H. g. Huang, R. X. Tan, R. Zhu, Y. Liu and Z. J. Wang, *RSC Adv.*, 2023, **13**, 20876–20888.
- 7 J. Zhang, L. J. Pei, J. Wang, P. Q. Zhu, X. M. Gu and Z. F. Zheng, *Catal. Sci. Technol.*, 2020, **10**, 1518–1528.
- 8 K. Rajendran, N. Pandurangan, C. P. Vinod, T. S. Khan, S. Gupta, M. A. Haider and D. Jagadeesan, *Appl. Catal., B*, 2021, **297**, 120417.
- 9 S. L. Zhao, D. W. Wang, R. Amal and L. M. Dai, *Adv. Mater.*, 2018, **31**, 1801526.
- 10 G. W. Geng, P. L. Chen, B. Guan, L. Jiang, Z. F. Xu, D. W. Di, Z. Y. Tu, W. C. Hao, Y. P. Yi, C. C. Chen, M. H. Liu and W. P. Hu, *ACS Nano*, 2017, **11**, 4866–4876.
- 11 W. C. Wan, Y. G. Zhao, J. Meng, C. S. Allen, Y. Zhou and G. R. Patzke, *Small*, 2023, 2304663.
- 12 H. Q. Qu, B. Li, Y. R. Ma, Z. Y. Xiao, Z. G. Lv, Z. J. Li, W. Li and L. Wang, *Adv. Mater.*, 2023, **35**, 2301359.
- 13 X. F. Luo, Y. X. Zhai, P. Wang, B. Tian, S. X. Liu, J. Li, C. H. Yang, V. Strehmel, S. J. Li, K. Matyjaszewski, G. Yilmaz, B. Strehmel and Z. J. Chen, *Angew. Chem., Int. Ed.*, 2023, 1–59.
- 14 P. B. Cui, L. J. Zhao, Y. D. Long, L. M. Dai and C. G. Hu, *Angew. Chem., Int. Ed.*, 2023, **62**, 202218269.
- 15 L. H. Zhang, Y. M. Shi, Y. Wang and N. R. Shiju, *Adv. Sci.*, 2020, **7**, 1902126.
- 16 Y. Cheng, H. C. Wang, T. Qian and C. L. Yan, *EnergyChem*, 2022, **4**, 100074.



- 17 M. L. Chen, J. F. Kou, H. W. Ma, Y. S. Xiang, P. Ma, L. M. Sun, X. C. Zhan, J. Y. Zhang, H. Zhang, F. S. Wang and Z. P. Dong, *Phys. Chem. Chem. Phys.*, 2023, **25**, 4201–4210.
- 18 K. B. Zhang, Z. Y. Wang, X. Y. Liu, G. Yang, C. Y. Jiang, Z. C. Pan, X. N. Liu, Y. Wang and B. Xing, *Environ. Sci.: Water Res. Technol.*, 2024, **10**, 376–388.
- 19 A. Khan, M. Goepel, J. C. Colmenares and R. Gläser, *ACS Sustain. Chem. Eng.*, 2020, **8**, 4708–4727.
- 20 W. Ding, Z. Wei, S. Chen, X. Qi, T. Yang, J. Hu, D. Wang, L. J. Wan, S. F. Alvi and L. Li, *Angew. Chem., Int. Ed.*, 2013, **52**, 11755–11759.
- 21 G. Z. Li, S. Y. Zheng, L. Wang and X. W. Zhang, *ACS Omega*, 2020, **5**, 7519–7528.
- 22 C. G. Hu and L. M. Dai, *Adv. Mater.*, 2019, **31**, 1804672.
- 23 C. J. Liao, B. Liu, Q. Chi and Z. H. Zhang, *ACS Appl. Mater. Interfaces*, 2018, **10**, 44421–44429.
- 24 J. Lv, Y. F. Zheng, Y. Y. Zhu, M. Yuan, Y. L. Chang and Z. P. Dong, *ChemistrySelect*, 2019, **4**, 4083–4091.
- 25 J. X. Shan, X. Q. Sun, S. Y. Zheng, T. D. Wang, X. W. Zhang and G. Z. Li, *Carbon*, 2019, **146**, 60–69.
- 26 W. Xiong, Z. N. Wang, S. L. He, F. Hao, Y. Z. Yang, Y. Lv, W. B. Zhang, P. L. Liu and H. A. Luo, *Appl. Catal., B*, 2020, **260**, 118105.
- 27 P. R. Thombal, K. M. Rao, S. M. Zo, K. B. Narayanan, R. S. Thombal and S. S. Han, *Catal. Lett.*, 2021, **152**, 538–546.
- 28 Z. Y. Xia, B. W. Wang, J. Y. Li, F. Y. Zhang, L. G. Chen and Y. Li, *New J. Chem.*, 2023, **47**, 5621–5624.
- 29 S. Chen, H. M. Xie and G. L. Zhou, *Ceram. Int.*, 2019, **45**, 24609–24617.
- 30 X. R. Liu, M. Zhang, D. N. Yu, T. Li, M. Wan, H. Zhu, M. L. Du and J. M. Yao, *Electrochim. Acta*, 2016, **215**, 223–230.
- 31 H. L. Chu, C. F. Shao, S. J. Qiu, Y. J. Zou, C. J. Xiang, F. Xu and L. X. Sun, *Inorg. Chem. Front.*, 2018, **5**, 225–232.
- 32 X. Y. Lu, D. Wang, L. P. Ge, L. H. Xiao, H. Y. Zhang, L. L. Liu, J. Q. Zhang, M. Z. An and P. X. Yang, *New J. Chem.*, 2018, **42**, 19665–19670.
- 33 D. R. Zeng, X. Yu, Y. F. Zhan, L. M. Cao, X. X. Wu, B. D. Zhang, J. L. Huang, Z. P. Lin, F. Y. Xie and W. H. Zhang, *Int. J. Hydrogen Energy*, 2016, **41**, 8563–8575.
- 34 X. W. Hu, Y. Long, M. Y. Fan, M. Yuan, H. Zhao, J. T. Ma and Z. P. Dong, *Appl. Catal., B*, 2019, **244**, 25–35.

